Supporting information for

Non-thermal Plasma Catalysis Driven Sustainable Pyrolysis Oil Upgrading to Jet Fuel at Near Ambient Conditions

Hoang M.Nguyen,[a] Ali Omidkar,[a] Wenping Li,[a] Zhaofe Li,[a] Hua Song*[a]

[a]Green Catalysis Research Group, Department of Chemical and Petroleum Engineering, University of Calgary, 2500 University Dr NW, Calgary, AB T2N 1N4, Canada.

Corresponding author:

E-mail address: sonh@ucalgary.ca (Prof. Hua Song).

Table of content of supporting information

Calculation details

Methane conversion:

$$CH_4 = 1 - \frac{mol_{CH_4}^{out}}{mol_{CH_4}^{in}} \times 100\%$$

Where, $mol_{CH_4}^{in}$ and $mol_{CH_4}^{out}$ are the input and output mole of CH_4 (mol), respectively.

Mass balance and product yields:

$$Total\ mass\ balance\ = \frac{\sum_{mass}(gas + liquid + solid_{after\ reaction})}{\sum_{mass}(gas + liquid + solid_{before\ reaction})} \times 100\%$$

$$Liquid\ Yield\ (\%) = \frac{Mass\ of\ producted\ liquid\ (g)}{Mass\ of\ CH_4(g) + Mass\ of\ feed\ oil\ (g)} \times 100\%$$

$$Mass\ of\ coke\ (\%) = \frac{Mass\ of\ coke}{Mass\ of\ inlet\ CH_4(g) + Mass\ of\ feed\ oil\ (g)} \times 100\%$$

$$Gas\ Yield\ (\%) = 100 - Liquid\ yield\ (\%) - coke\ yield\ (\%)$$

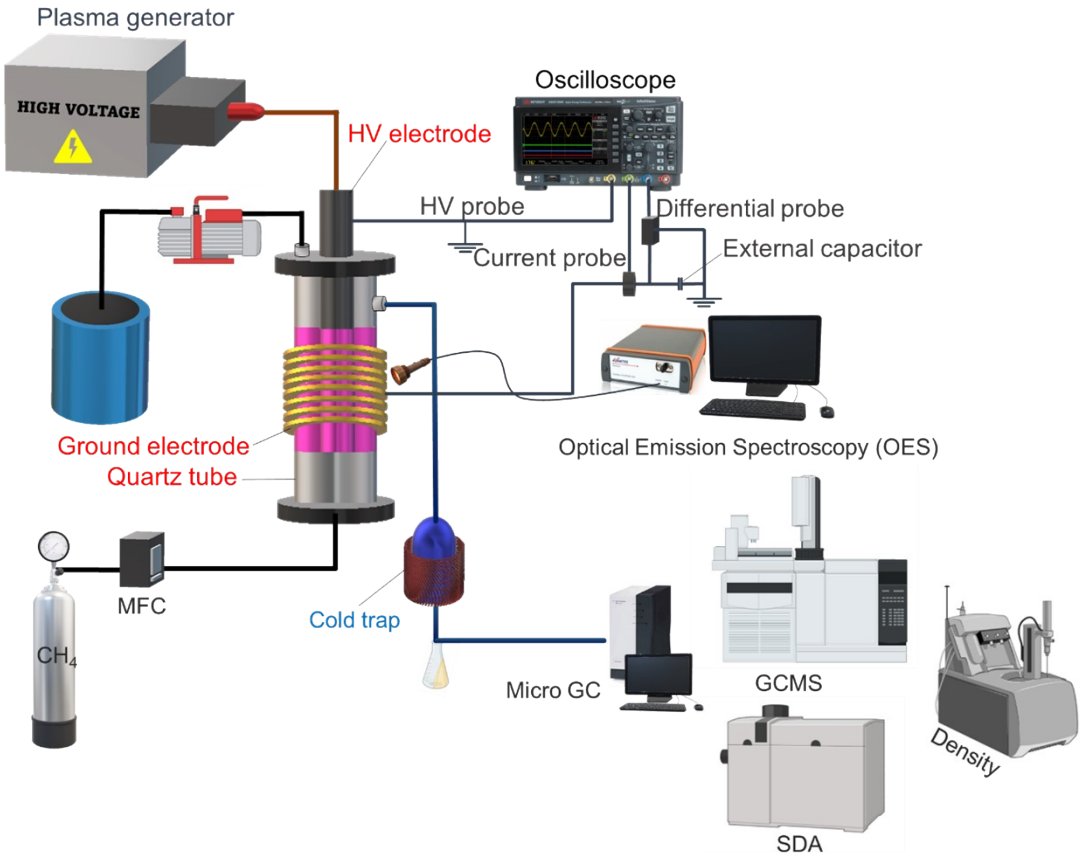

Fig.S1. Schematic diagram of triphase plasma catalytic driven pyrolysis oil upgrading to jet fuel.

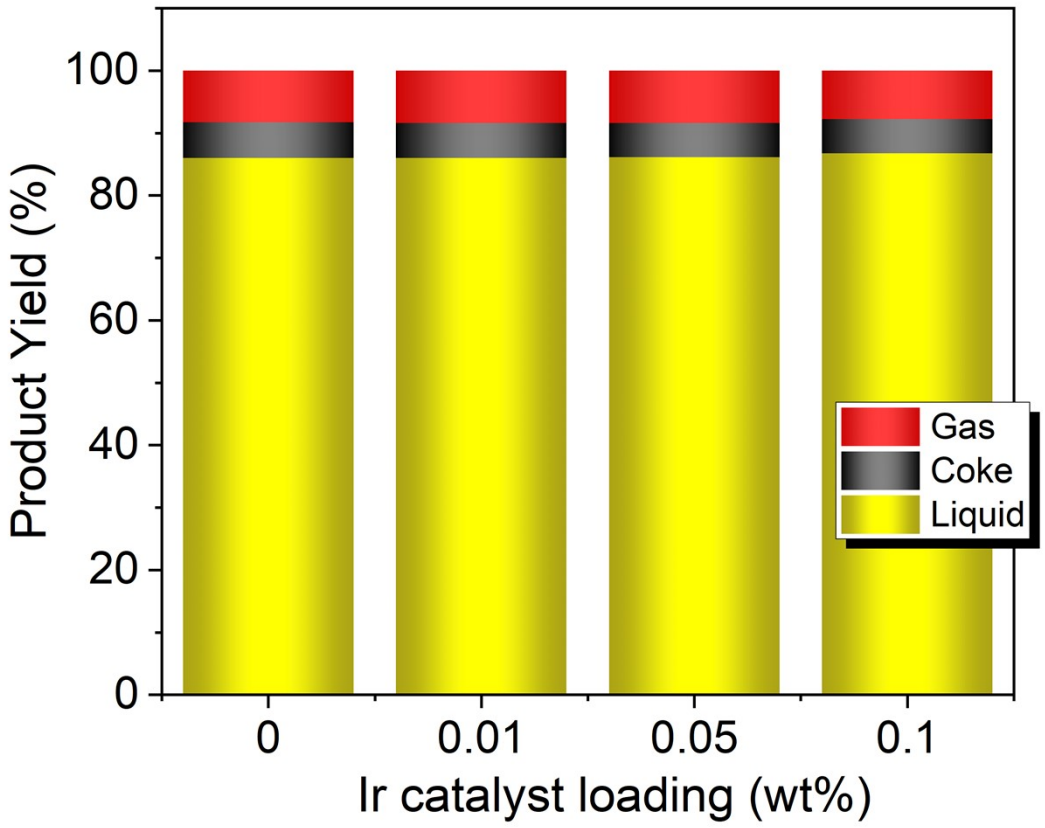

Fig.S2. Effects of Ir catalyst loadings on the product yields.

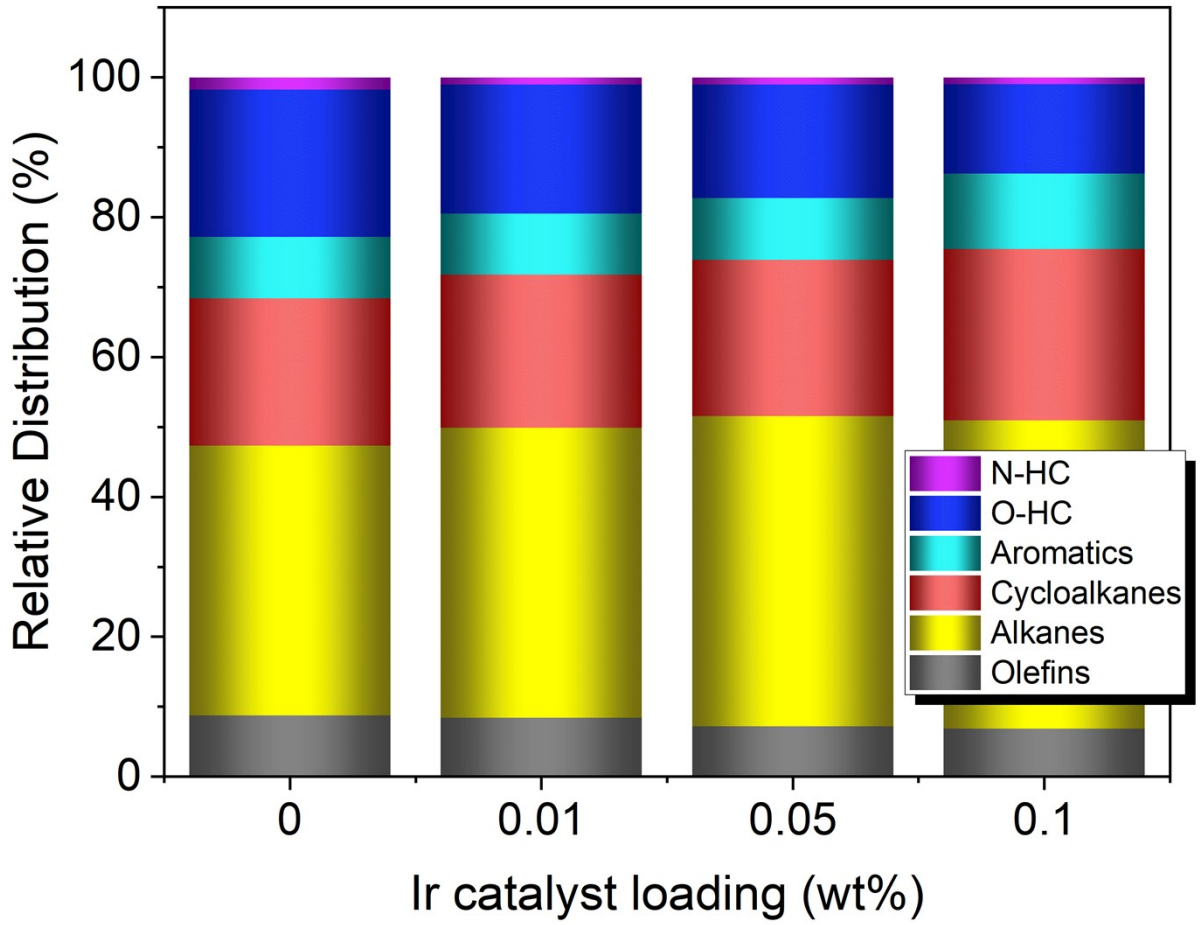

Fig.S3. Effects of Ir catalyst loadings on the relative distribution of products.

Table S1. Textural properties of the GaN, fresh and spent Ir/GaN samples.

Catalyst	BET Surface Area ($m^2\ g^{-1}$)	Pore Volume ($cm^3 g^{-1}$)	Pore Size (nm)
GaN	8.0	0.031	19.0
Fresh Ir-GaN	14.6	0.052	14.5
Spent Ir-GaN	23.1	0.098	11.8

Table S2. Molecular weight of feed and upgraded oils.

Oil	**Molecular weight (g mol^{-1})**
Feed	210.0
Upgraded with Empty tube	181.2
Upgraded with GaN	171.2
Upgraded with Ir/GaN	165.6

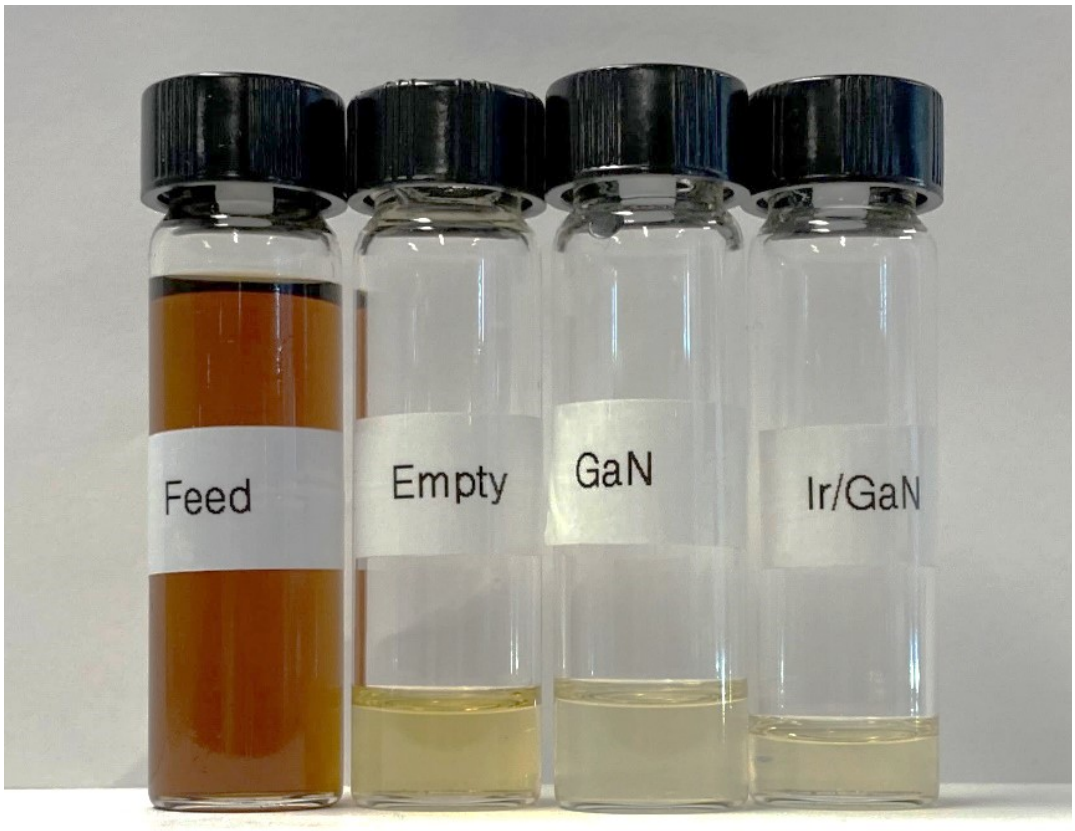

Fig.S4. Containers of feed and upgraded oils produced from different triphase plasma driven reactions. [Reactions conditions: Plasma power: 12W; CH_4 flowrate of 100 cm^3 min^{-1}; oil flowrate: 0.05 cm^3 min^{-1}].

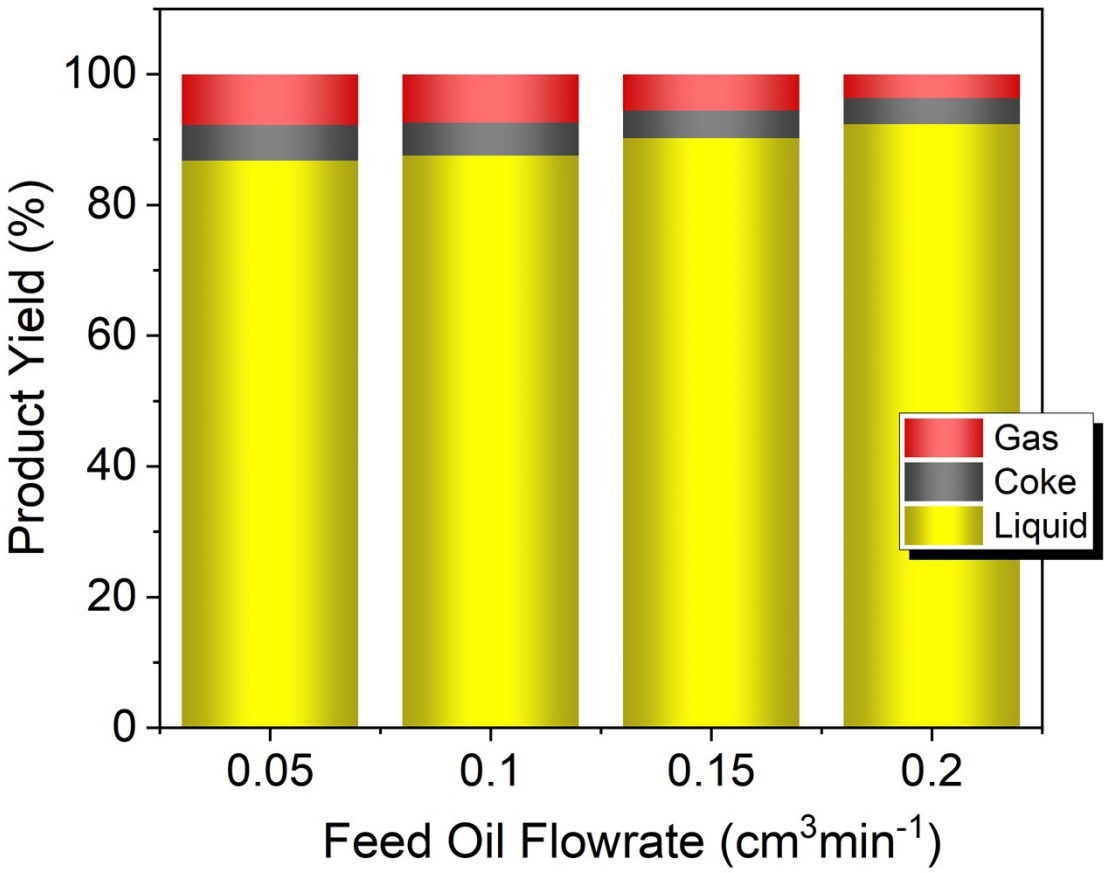

Fig.S5. Effects of feed oil flowrates on the product yields.

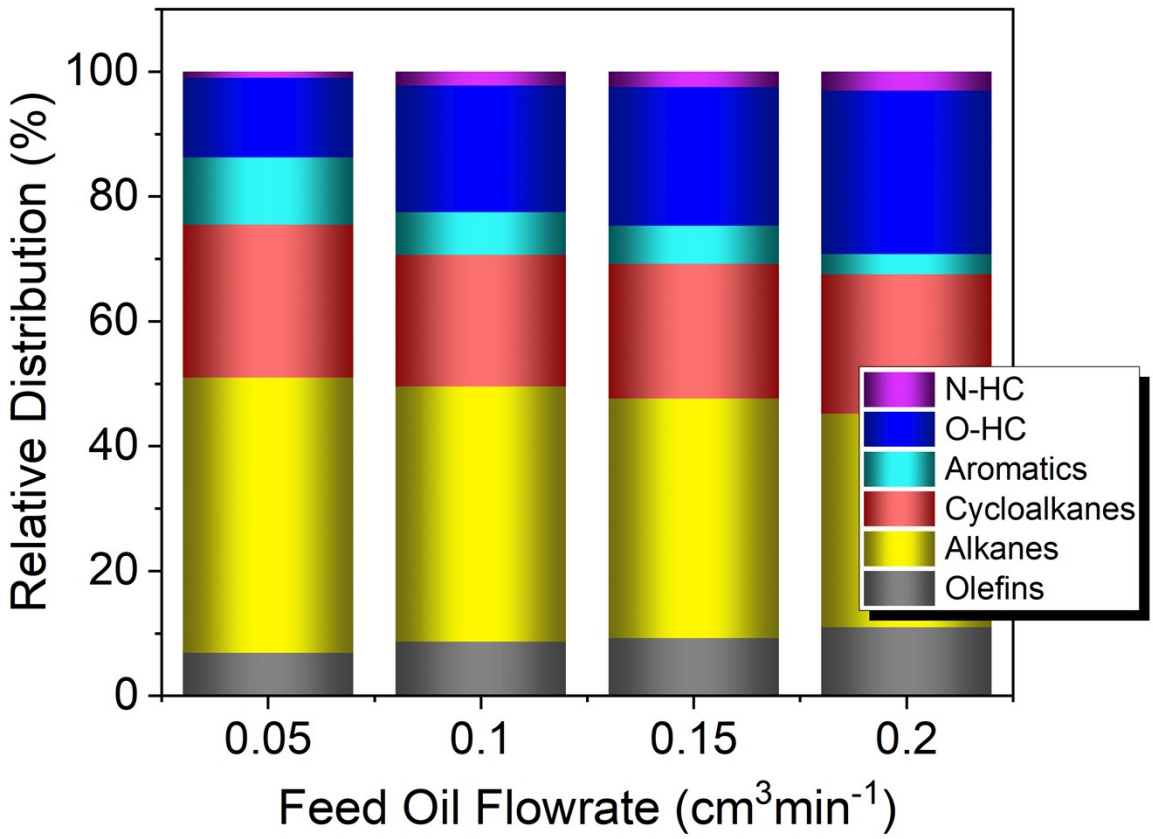

Fig.S6. Effects of feed oil flowrates on the relative distribution of products.

Table S3. Comparison of upgrading heavy hydrocarbons to jet fuel range hydrocarbons between thermal catalytic processes and this work.

Feedstock	Catalyst	Gas	Reactor	Reaction conditions				Oil yield (%)	Remark	Ref.
				T (^oC)	P bar	T (h)	W_{cat} (g)			
Guaiacol	$Pd_{2\%}/H_\beta$	H_2	Batch	220	30	4	0.03	77.66	- At a low reaction temperature of 160 °C, the predominant hydrocarbon product was cyclohexane. - When the H_2 pressure was set at 5 and 10 bar, the conversion of guaiacol was merely 2.96% and 8.04%, respectively. This indicates that a high-pressure environment was essential to facilitate the generation of active hydrogen required for breaking the C-O bonds in the hydrodeoxygenation process.	[1]
α-tetralone	Pd-Ni/SBA-16	H_2	Continuous fixed-bed down-flow reactor	400	1	12	0.06	88.21	- The catalytic activity of Pd-Ni impregnated on various supports, including different mesoporous materials (MCM-41, SBA-15, KIT-6) and metal oxides	[2]

									(γ-Al_2O_3, CeO_2, TiO_2, ZrO_2, SiO_2), was compared with that of Pd-Ni/SBA-16. - The observed catalytic activity exhibited the following order: SBA-16 >KIT-6>SBA-15>MCM-41>γ-Al_2O_3>SiO_2> CeO_2 >TiO_2>ZrO_2. - Mesoporous materials with high surface area, thermal stability, and evenly dispersed metals displayed higher catalytic activity compared to metal oxides.	
Isoeugenol	Pt (4 wt%)-Re (4 wt%)/ Sibunit	H_2	Batch (thermal reactor)	250	30	4	0.05	84.0	-The two primary products were 2-methoxy-4-propylcyclohexanol, obtained through the hydrogenation of the aromatic ring, and propylcyclohexane (the desired product), resulting from both the hydrogenation of the aromatic ring and complete deoxygenation. -The monometallic Pt catalyst exhibited low activity. However, the	[3]

									incorporation of Re (rhenium) to create a bi-metallic catalyst (Pt-Re/Sibunit) had a significant impact on hydrodeoxygenation activity. In this case, ReO_x introduced oxygen vacancies crucial for the deoxygenation process.	
Cyclohexanone	Sulfided CoMo/γ-Al_2O_3	N_2 and H_2 (50%–50%)	Continuous-fixed-bed flow reactor	350	8	6	2	n.a	- Elevated pressures within the investigated range of 8–20 bar were found to enhance selectivity towards deoxygenated products, such as benzene and cyclohexene. - Concurrently, an overall conversion improvement from 7% to 18% was observed as the temperature increased from 300 to 350 °C.	4
Waste cooking oil	$ZnAl_2O_4$	H_2	Batch reactor	450	120	1	n/a	80	- Elevated pressures within the investigated range of 8–20 bar was found to enhance selectivity towards deoxygenated products, such as benzene and cyclohexene. - Concurrently, an overall conversion improvement	5

									from 7% to 18% was observed as the temperature increased from 300 to 350 °C.	
Phenol + benzyl acetate	5 wt.% Pd/C and Montmorillonite	H_2	Batch-autoclave reactor (MMT)	180	60	10	2.3	75.2	- Benzylphenols were synthesized through the alkylation of phenol and benzyl acetate utilizing an MMT catalyst. Hydrodeoxygenation of the alkylation products was performed over a Pd/C catalyst to yield hydrocarbons within the jet fuel range. -The primary alkylation products were identified as 2-benzylphenol and 4-benzylphenol, achieving a 70% yield at 140°C with a reaction time of 2h. - Reducing the reaction temperature from 220 to 180 °C led to an increase in the yield of perhydrofluorene (from 34.36% to 75.20%). In contrast, the yield of dicyclohexylmethane decreased (from 50.96% to 10.42%). This change is attributed to the	[6]

									saturation of two benzene rings in 2-benzylphenol and 4-benzylphenol through simultaneous hydrogenation at the higher reaction temperature, thereby suppressing the intramolecular alkylation reaction.	
Propanal	$Cu/SiO_2–TiO_2$ (upstream catalyst) Ni/ZSM-5 (downstream catalyst)	H_2	Continuous dual-bed fixed-bed reactor	300	10	5	2	n.a	- A dual-bed reactor was employed as a strategic solution to tackle challenges associated with the hydrodeoxygenation of small oxygenates, wherein they undergo hydrogenation to produce light hydrocarbons. The dual-bed catalyst demonstrated significantly higher efficacy, resulting in an 81.7% yield of jet fuel range hydrocarbons compared to the single-bed counterpart ($Cu/SiO_2–TiO_2$) with a yield of 12.3%. - In the dual-bed setup, propanal initially engaged with the	7

									upstream catalyst ($Cu/SiO_2–TiO_2$), leading to enhanced chain growth, predominantly yielding C_9 ketone. -This configuration effectively curtailed side reactions, particularly the generation of olefins via the direct dehydration of propanal, when compared to the Ni/HZSM-5 catalyst.	
Biomass-derived pyrolysis oil	0.1wt% Ir/GaN	CH_4	Continuous fluidized bed reactor	100	1	24	0.1	87.0	- Showcase of an efficient H_2-free pyrolysis oil upgrading process using a triphase plasma catalytic system. - Impressive oil yields reaching nearly 87%, with density and viscosity meeting ASTM standards. - Product distribution, including alkanes, cycloalkanes, and aromatics, aligns with commercial jet fuel requirements. - Achieved under mild operating conditions: temperatures around 100°C and ambient	This work

pressure.

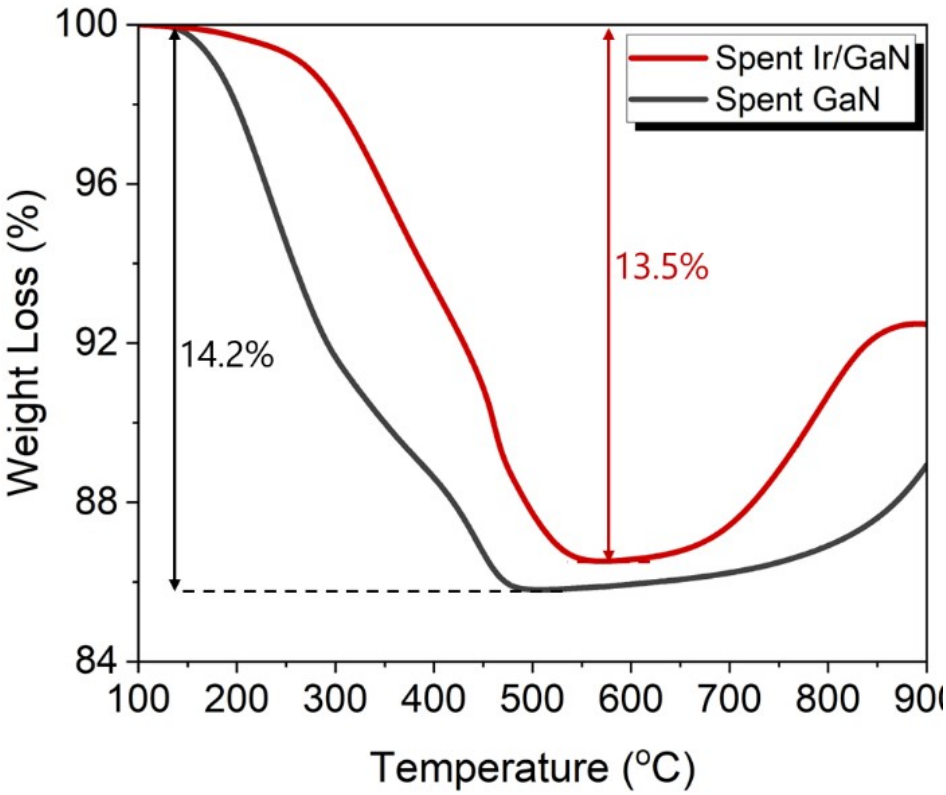

Fig.S7. TGA profile of spent GaN and Ir/GaN catalysts.

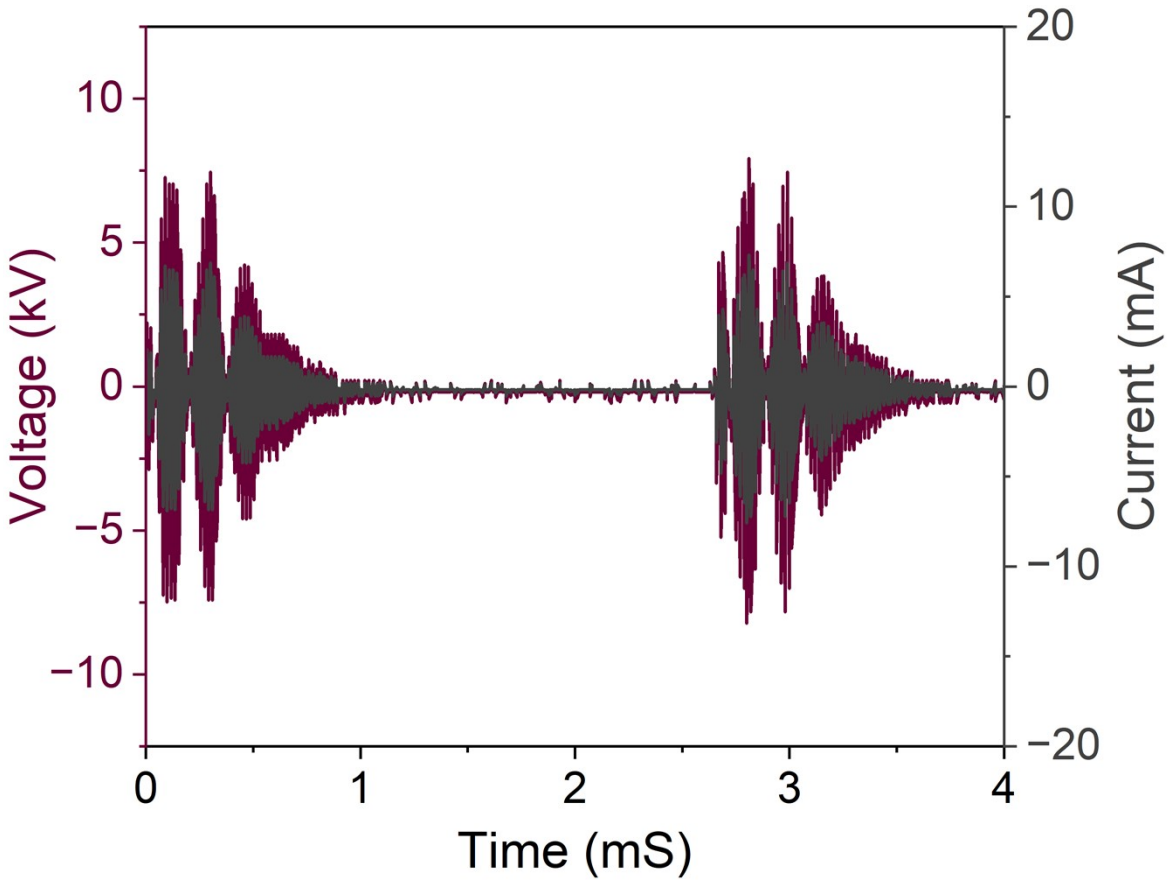

Fig. S8. Voltage-Current profile of plasma discharge inside triphase pyrolysis oil upgrading.

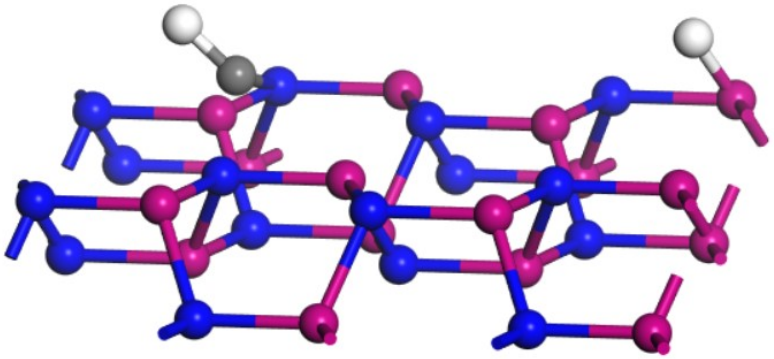

Fig. S9. Possible structure and adsorption of CH and H species on the GaN (110) surface.

Table S4. Adsorption energy diagram for CH_4 dissociation on the GaN (110) and Ir (100) under plasma regime.

Reaction steps	**Adsorption energy (eV)**	
	GaN	**Ir**
CH_4	-0.23	-0.06
$CH_4 \rightarrow CH_3 + H$	-0.41	-0.24
$CH_4 \rightarrow CH_2 + 2H$	-0.5	-0.3
$CH_4 \rightarrow CH + 3H$	-0.54	-0.36
$CH_4 \rightarrow C + 4H$	-0.64	-0.42

References

1. L. Hu, X.-Y. Wei, M.-L. Xu, Y.-H. Kang, X.-H. Guo, F.-B. Zhang, Z.-M. Zong and H.-C. Bai, *J. Environ. Chem. Eng*, 2021, **9**, 106599.
2. G. Vijayakumar and A. Pandurangan, *Energy*, 2017, **140**, 1158-1172.
3. M. E. Martínez-Klimov, P. Mäki-Arvela, Z. Vajglova, M. Alda-Onggar, I. Angervo, N. Kumar, K. Eränen, M. Peurla, M. H. Calimli, J. Muller, A. Shchukarev, I. L. Simakova and D. Y. Murzin, *Energy Fuels*, 2021, **35**, 17755-17768.
4. M. Saidi and A. Jahangiri, *Chem. Eng. Res. Des.*, 2017, **121**, 393-406.
5. R. El-Araby, E. Abdelkader, G. El Diwani and S. I. Hawash, *Bull. Natl. Res. Cent* . 2020, **44**, 177.
6. J. Bai, Y. Zhang, X. Zhang, C. Wang and L. Ma, *ACS Sustain. Chem. Eng.*, 2021, **9**, 7112-7119.
7. I. Yeboah, X. Feng, G. Wang, K. R. Rout, Z. Cai, X. Duan, X. Zhou and D. Chen, *ACS Sustain. Chem. Eng.*, 2020, **8**, 9434-9446.